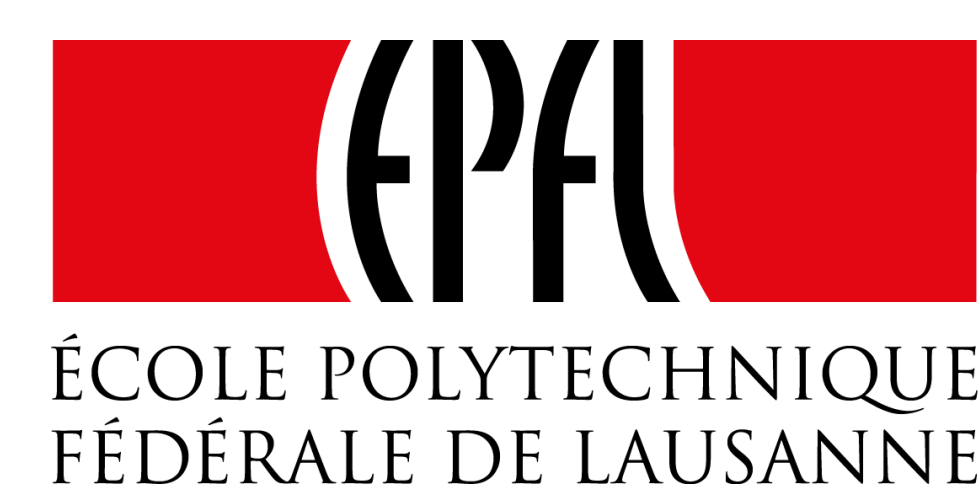


Turbulence simulations in diverted geometry

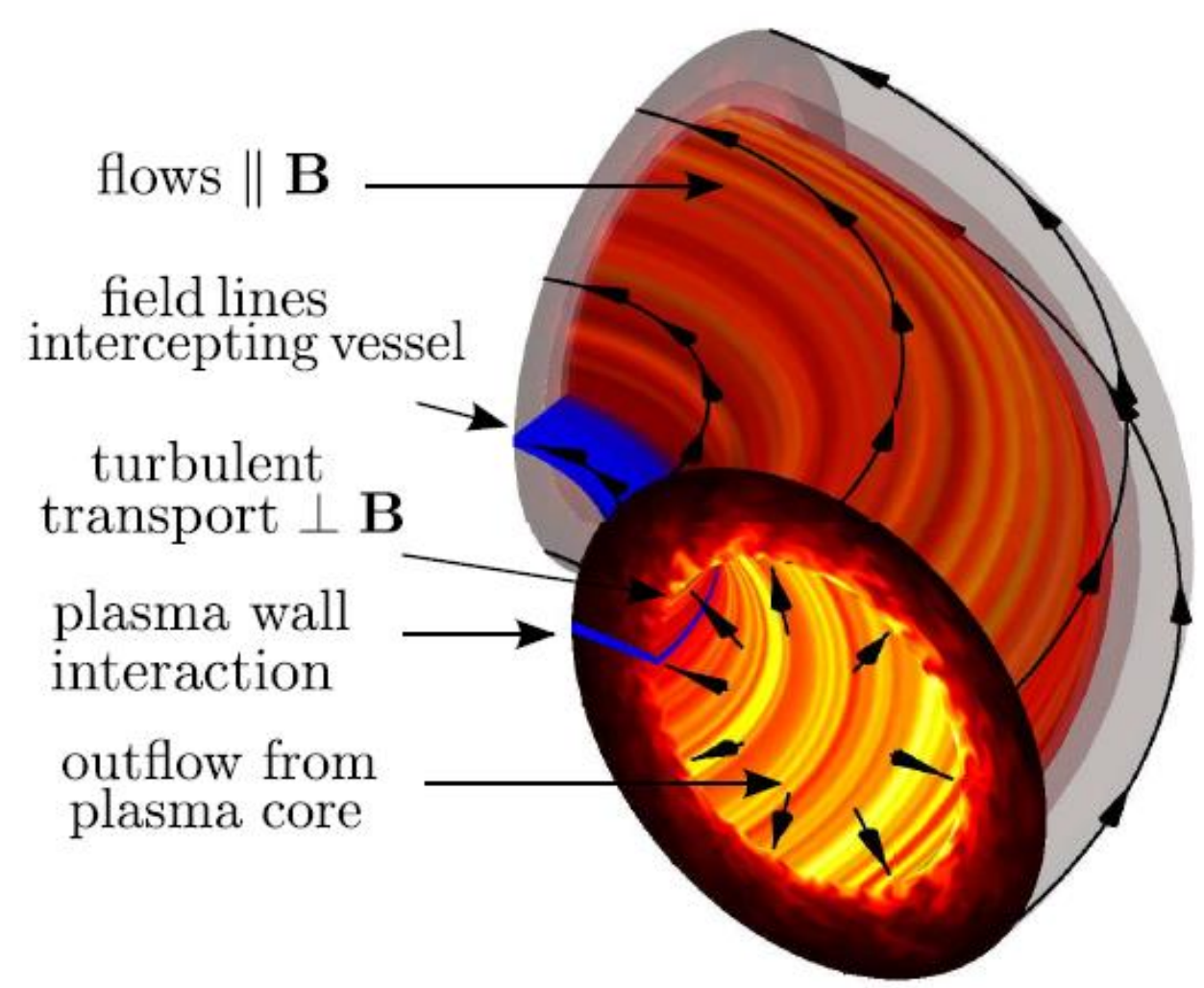
M. Giacomini, P. Ricci, C. Beadle, A. Corrado, P. Paruta

École Polytechnique Fédérale de Lausanne (EPFL), Swiss Plasma Center (SPC), CH-1015 Lausanne, Switzerland



SWISS PLASMA
CENTER

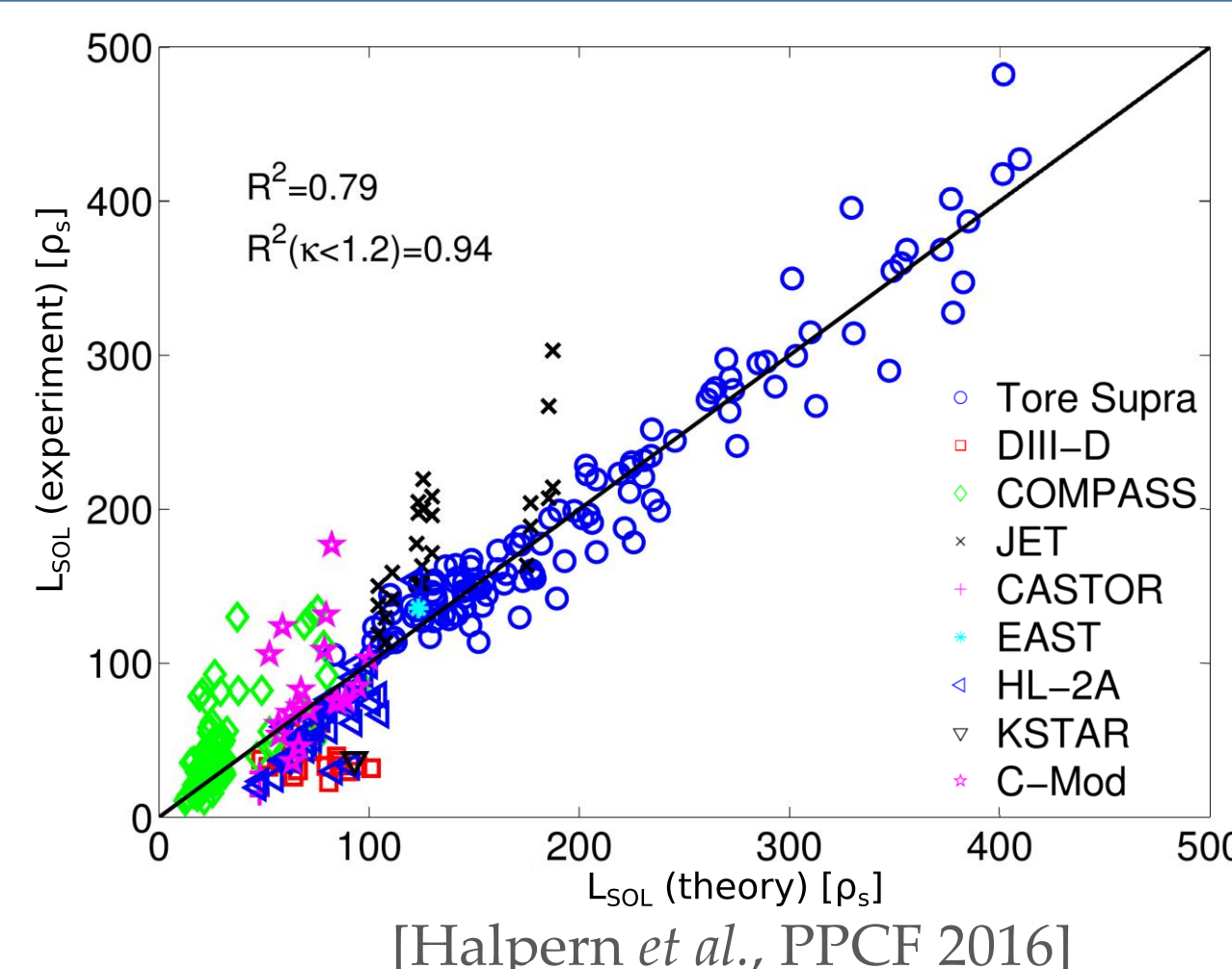
The tokamak periphery and GBS code



- The **tokamak periphery** is divided in two parts: the plasma **edge** and the **Scrape-Off Layer (SOL)**
- The **edge** is the plasma region between the core and the last closed flux surface (**LCFS**)
- The **turbulence across the LCFS** determines the **confinement**
- The **SOL** is the plasma region **outside the LCFS**
- In the **SOL**, **magnetic field lines intersect the walls of the fusion device**
- **Heat and particles** flow along magnetic field lines and **are exhausted to the vessel**
- **Global Braginskii Solver (GBS) Code** is a 3D, flux-driven, global turbulence code in **limited and diverted X-point** configurations used to study plasma **turbulence in the tokamak periphery** [Halpern et al., JCP 2016], [Ricci et al. PPCF 2012]
- GBS solves 3D fluid equations for electrons and ions, Poisson's and Ampere's equations, and a kinetic equation for neutral atoms

Some of the past GBS achievements

- Characterization of non-linear turbulent regimes in the SOL [Masetto et al., PoP 2013]
- SOL width scaling as a function of dimensionless/engineering plasma parameters [Halpern et al., PPCF 2016]
- Origin and nature of intrinsic toroidal plasma rotation in the SOL [Loizu et al., PoP 2014]
- Mechanisms regulating the SOL equilibrium electrostatic potential [Loizu et al., PPCF 2013]



A new version of GBS for diverted geometry

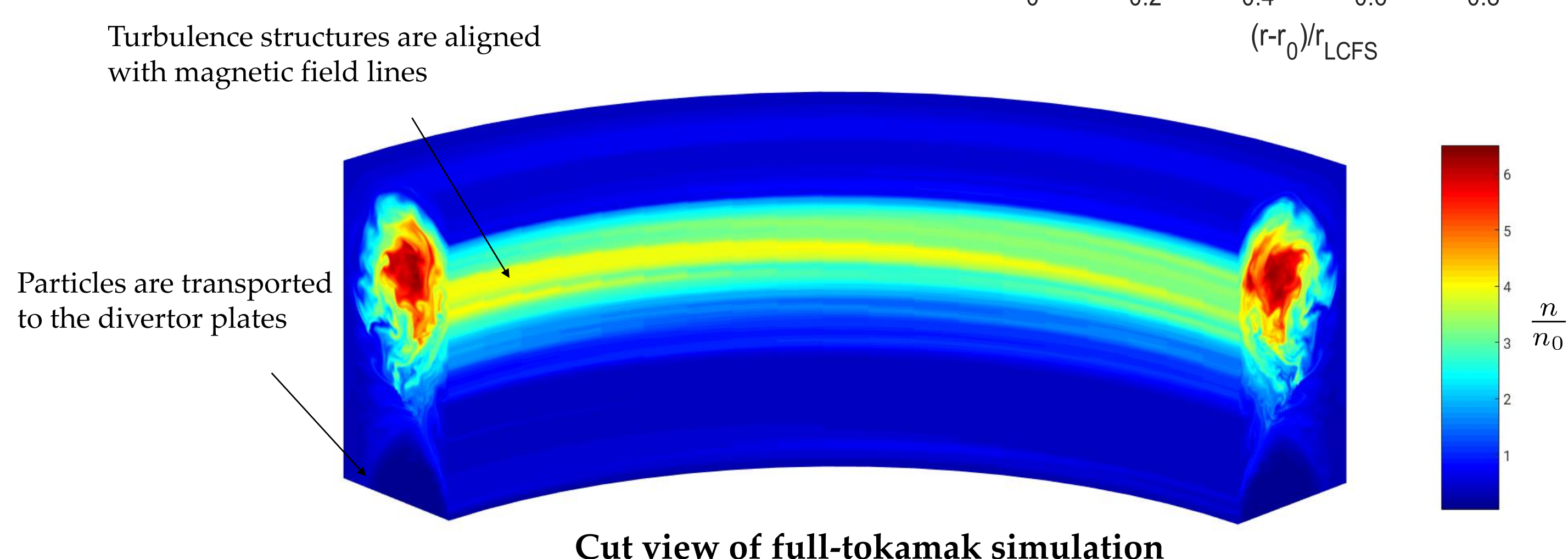
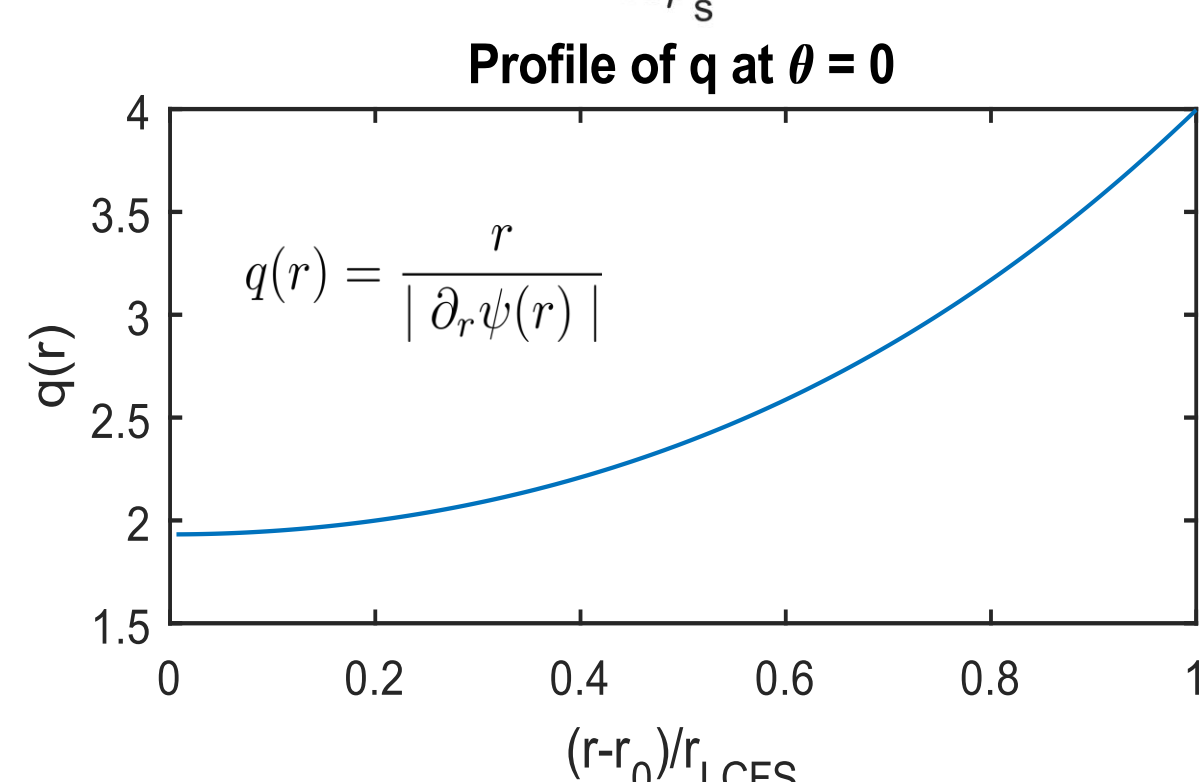
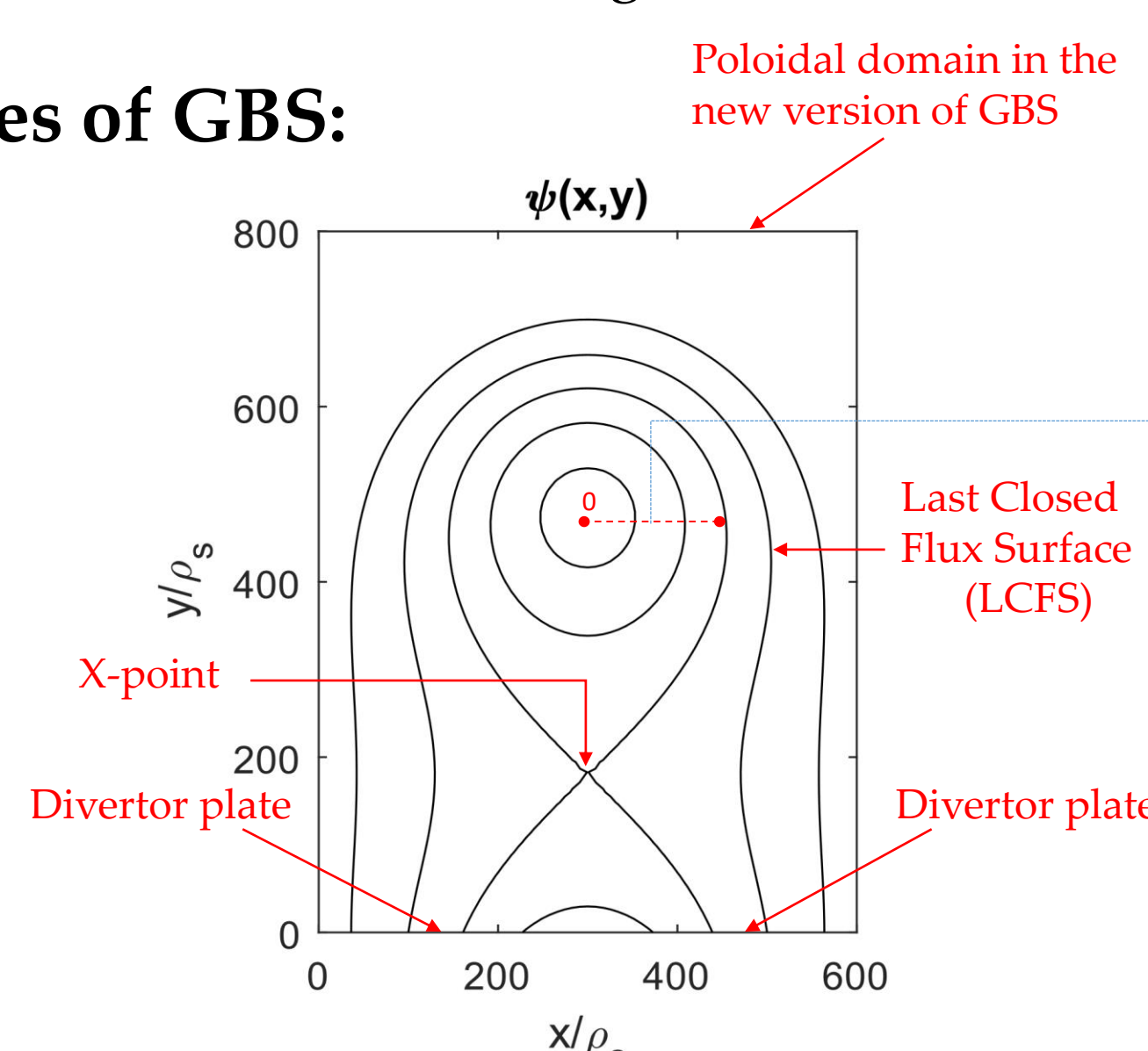
Numerical implementation in GBS:

[Paruta et al., submitted to PoP]

- Spatial accuracy: **4th order centered finite differences** scheme with the grid **staggered in the toroidal and vertical direction**
- An extension to the **4th order of the Arakawa algorithm** is used for the Poisson bracket operator $[\phi, f]$
- Time evolution: **4th order Runge-Kutta** time stepping method
- **Non-field-aligned coordinate system** is used to treat diverted configurations

The new main features of GBS:

- **Full-tokamak simulations** to investigate the interaction between core and edge: **boundary conditions at the core are no longer needed**
- Rectangular poloidal domain guarantees much **more flexibility on the geometry size** (it reduces computational domain in SOL)
- **More flexibility** in choosing the **magnetic poloidal flux** as a function of x and y cartesian coordinates
- Proper boundary conditions are applied to the **divertor plates**. A **Robin boundary condition** for the **electric potential** is used



Conclusion and future plans

Conclusion

- **Full-tokamak** simulations used to investigate the **core-edge turbulence transport**
- Analysis of the **electric potential** in the tokamak (SOL, edge and core)
- Formation of $\vec{v}_{E \times B}$ shear and preliminary study of the **L-H mode transition**.

Next steps

- Expand the **analysis** with the simplified **time and toroidal averaged equation**
- Determination of the **heat flux** impacting on the **divertor plates**
- Effect of core-edge **turbulence transport** on **SOL width**

Drift-reduced fluid equations implemented in GBS

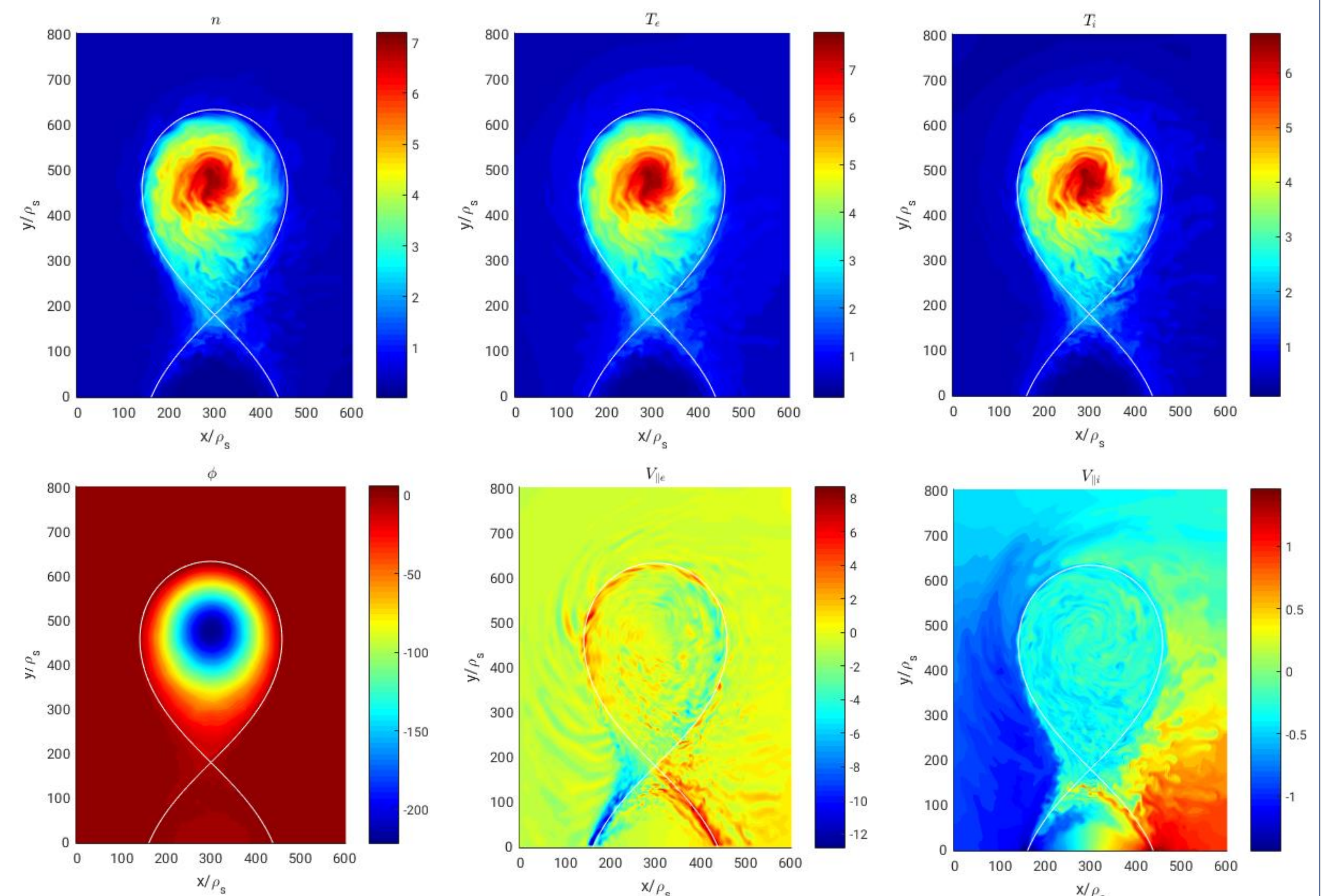
- GBS evolves the **drift-reduced Braginskii equations** with ordering $k_{\parallel} \ll k_{\perp}$ and $d/dt \ll \omega_{ci}$
- Plasma and heating outflowing from the wall is mimicked by localized plasma and heat sources S_n , S_{T_e} and S_{T_i}

$$\begin{aligned} \frac{\partial n}{\partial t} &= -\frac{1}{B} \frac{R_0}{\rho_{s0}} [\phi, n] + \frac{2}{B} [C(p_e) - nC(\phi)] - \nabla_{\parallel} (nv_{\parallel e}) + D_n \nabla_{\perp}^2 n + S_n \\ \frac{\partial \omega}{\partial t} &= -\frac{1}{B} \frac{R_0}{\rho_{s0}} [\phi, \omega] - v_{\parallel i} \nabla_{\parallel} \omega + \frac{B^2}{n} \nabla_{\parallel} j_{\parallel} + \frac{2B}{n} C(p_e + \tau p_i) + \frac{B}{3n} C(G_i) + D_{\omega} \nabla_{\perp}^2 \omega \\ \frac{\partial v_{\parallel e}}{\partial t} &= -\frac{1}{B} \frac{R_0}{\rho_{s0}} [\phi, v_{\parallel e}] - v_{\parallel e} \nabla_{\parallel} v_{\parallel e} + \frac{m_i}{m_e} \left(\nu j_{\parallel} + \nabla_{\parallel} \phi - \frac{1}{n} \nabla_{\parallel} p_e - 0.71 \nabla_{\parallel} T_e - \frac{2}{3n} \nabla_{\parallel} G_e \right) + D_{v_{\parallel e}} \nabla_{\perp}^2 v_{\parallel e} \\ \frac{\partial v_{\parallel i}}{\partial t} &= -\frac{1}{B} \frac{R_0}{\rho_{s0}} [\phi, v_{\parallel i}] - v_{\parallel i} \nabla_{\parallel} v_{\parallel i} - \frac{1}{n} \nabla_{\parallel} (p_e - \tau p_i) - \frac{2}{3n} \nabla_{\parallel} G_i + D_{v_{\parallel i}} \nabla_{\perp}^2 v_{\parallel i} \\ \frac{\partial T_e}{\partial t} &= -\frac{1}{B} \frac{R_0}{\rho_{s0}} [\phi, T_e] - v_{\parallel e} \nabla_{\parallel} T_e + \frac{4}{3} \frac{T_e}{B} \left[\frac{7}{2} C(T_e) + \frac{T_e}{n} C(n) - C(\phi) \right] + D_{T_e} \nabla_{\perp}^2 T_e + \chi_{\parallel e} \nabla_{\parallel}^2 T_e \\ &\quad + \frac{2}{3} T_e \left[0.71 \nabla_{\parallel} v_{\parallel i} - 1.71 \nabla_{\parallel} v_{\parallel e} + 0.71 (v_{\parallel i} - v_{\parallel e}) \frac{\nabla_{\parallel} n}{n} \right] + S_{T_e} \\ \frac{\partial T_i}{\partial t} &= -\frac{1}{B} \frac{R_0}{\rho_{s0}} [\phi, T_i] - v_{\parallel i} \nabla_{\parallel} T_i + \frac{4}{3} \frac{T_i}{B} \left[C(T_e) + \frac{T_e}{n} C(n) - C(\phi) \right] + \frac{2}{3} T_i (v_{\parallel i} - v_{\parallel e}) \frac{\nabla_{\parallel} n}{n} \\ &\quad - \frac{2}{3} T_i \nabla_{\parallel} v_{\parallel e} - \frac{10}{3} \frac{T_i}{B} C(T_i) + D_{T_i} \nabla_{\perp}^2 T_i + S_{T_i} \end{aligned}$$

$$\omega = \nabla_{\perp}^2 \phi, \quad [\phi, f] = \vec{b} \cdot (\nabla \phi \times \nabla f), \quad C(f) = \frac{B}{2} \left(\nabla \times \frac{\vec{b}}{B} \right) \cdot \nabla f, \quad \vec{b} = \frac{\vec{B}}{B}$$

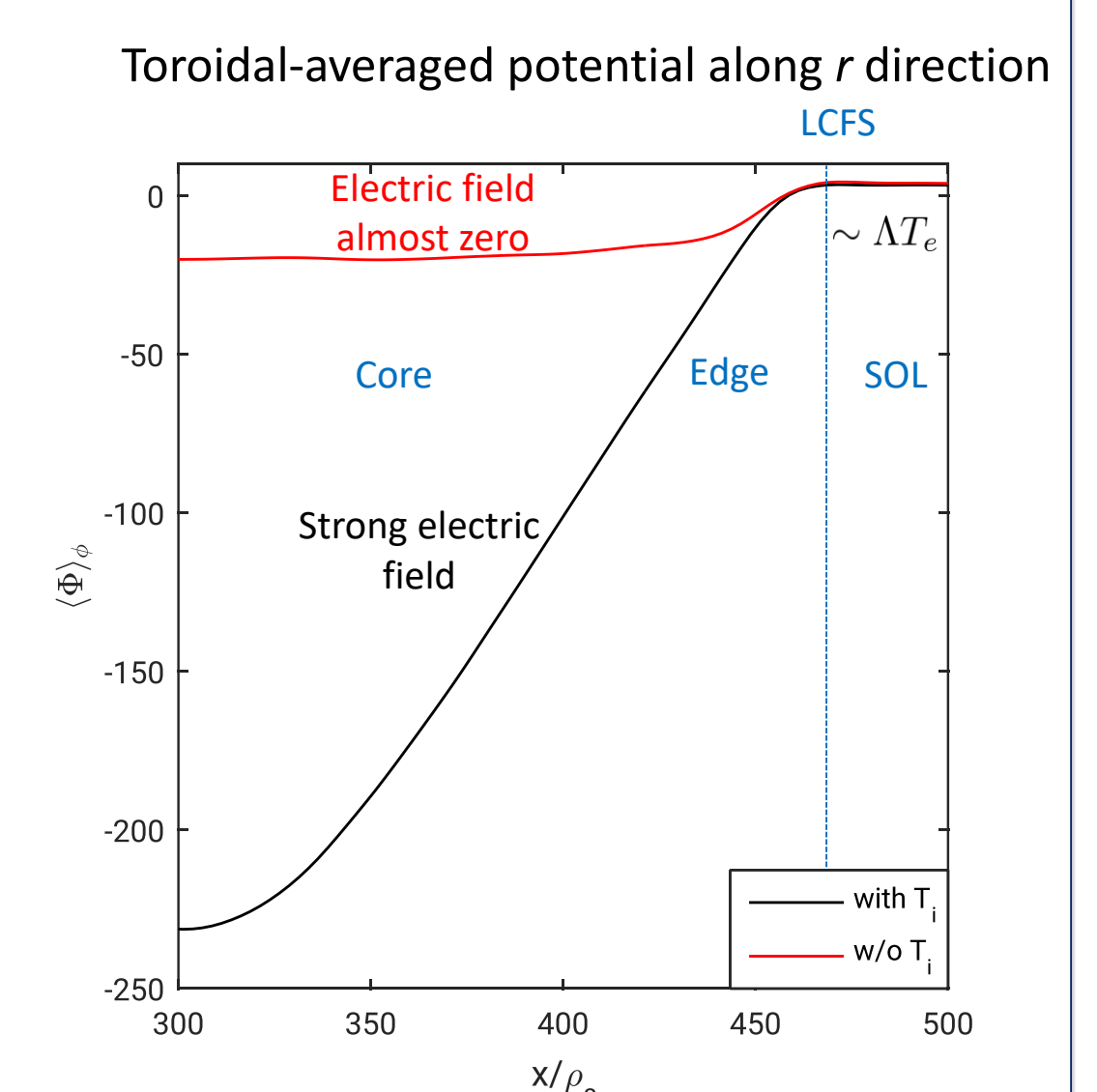
- System completed with **first-principles boundary conditions** applicable at the magnetic pre-sheath entrance [Loizu et al., PoP 2012]
- Normalized units used throughout: $L_{\perp} \rightarrow \rho_{s0}$, $L_{\parallel} \rightarrow R_0$, $t \rightarrow R_0/c_{s0}$, $v = n_0 R_0 e^2 / (m_i c_{s0} \sigma_{\parallel})$

Preliminary results



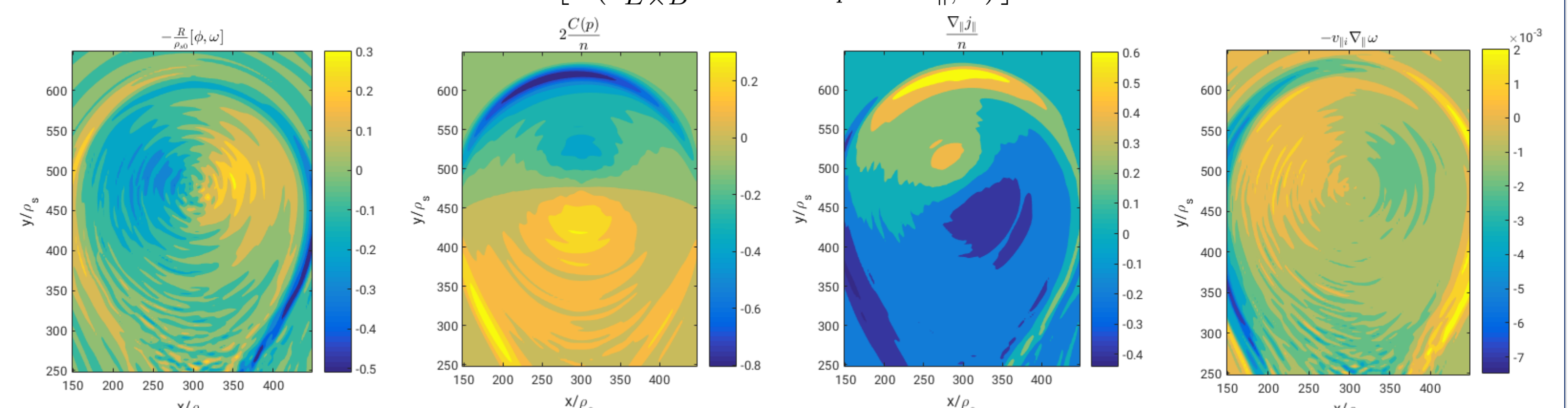
Electric potential in the tokamak

- In the **SOL**, the **electric potential follows the electron temperature** and it does not depend on the cold ion approximation.
- In the **edge and core**, the electric potential strongly depends on the ion temperature: in the **cold ion approximation no electric field** is generated
- The electric field leads to an $\vec{E} \times \vec{B}$ shear that **improves the plasma confinement**
- The analysis points out the importance of **ion heating** to reach a better confinement (**H-mode**). This result has been seen experimentally [F. Ryter et al., NC 2014]



- The $\vec{E} \times \vec{B}$ velocity is **self-generated** by the plasma when the ions are heated up: the **ion pressure gradient increases** as well as the **diamagnetic ion velocity** which is balanced by an increase of the $\vec{E} \times \vec{B}$ velocity
- By retaining only the dominant terms, the **time and toroidal averaged vorticity equation** (figures below) is $-\frac{R_0}{\rho_{s0}} n [\phi, \omega] + C(p_e + \tau p_i) + \nabla_{\parallel} j_{\parallel} \approx 0$
- By combining this equation with the **time and toroidal averaged density equation**, the **continuity equation for the ions is retrieved**, where \vec{v}_{pol} is the polarization velocity and it comes from the non-negligible term $-\frac{R_0}{\rho_{s0}} n [\phi, \omega]$

$$\nabla \cdot [n(\vec{v}_{E \times B} + \vec{v}_{di} + \vec{v}_{pol} + v_{\parallel i} \vec{b})] = 0$$



This work has been carried out within the framework of the EUROfusion Consortium and has received funding from the Euratom research and training programme 2014-2018 under grant agreement No 633053. The views and opinions expressed herein do not necessarily reflect those of the European Commission.

